Energy Materials

Supplementary Materials

Lithium-rich, oxygen-deficient spinel obtained through low-temperature decomposition of heterometallic molecular precursor

Yuxuan Zhang[1], Zheng Wei[1], Maria Batuk[2], Joke Hadermann[2], Alexander S. Filatov[3], Joyce Chang[1], Haixiang Han[4,*], Artem M. Abakumov[5,*], Evgeny V. Dikarev[1,*]

[1]Department of Chemistry, University at Albany, State University of New York, Albany, NY 12222, USA.

[2]EMAT, Department of Physics, University of Antwerp, Antwerp 2020, Belgium.

[3]Department of Chemistry, the University of Chicago, Chicago, IL 60637, USA.

[4]School of Material Science and Engineering, Tongji University, Shanghai 201804, China.

[5]Center for Energy Science and Technology, Skolkovo Institute of Science and Technology, Moscow 121205, Russia.

Correspondence to: Prof. Evgeny V. Dikarev, Department of Chemistry, University at Albany, State University of New York, 1400 Washington Ave, Albany, NY 12222, USA. E-mail: edikarev@albany.edu; Prof. Artem M. Abakumov, Center for Energy Science and Technology, Skolkovo Institute of Science and Technology, Nobel Str. 3, Moscow 121205, Russia. E-mail: a.abakumov@skoltech.ru; Prof. Haixiang Han, School of Materials Science and Engineering, Tongji University, 4800 Cao'an Road, Shanghai 201804, China. E-mail: hxhan@tongji.edu.cn

TABLE OF CNTENTS

X-ray powder diffraction pattern of heterometallic precursor 1

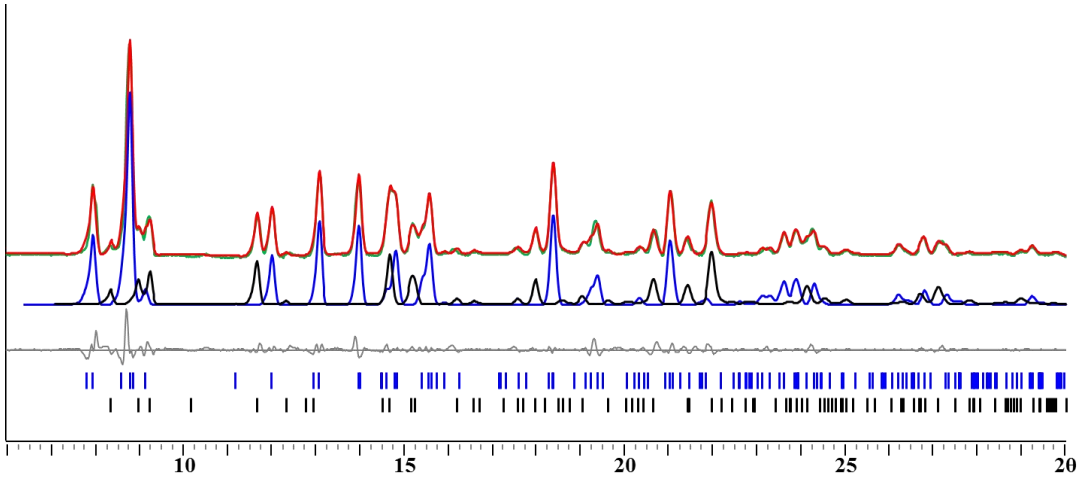

Figure S1. X-ray powder diffraction pattern of $Li_2Mn_2(tbaoac)_6$ (**1**) and the Le Bail fit. Red and green curves are experimental and calculated patterns overlaid. Blue and black curves are calculated single peak patterns for two polymorph modifications with theoretical peak positions shown at the bottom as blue and black lines (triclinic and monoclinic modifications, respectively). Grey line is the difference curve.

Table S1. Unit Cell Parameters of Complex 1 Obtained from Le Bail Fit and Single Crystal Data

$Li_2Mn_2(tbaoac)_6$ (1)			
	Le Bail fit (20 °C)		**Single crystal (-173 °C)**
Sp. Gr.	$P2_1/n$	P-1	P-1
a (Å)	12.104(2)	11.849(1)	11.758(2)
b (Å)	9.751(1)	12.748(2)	12.297(2)
c (Å)	19.220(2)	13.066(1)	12.536(2)
α (°)	90	104.299(3)	103.962(2)
β (°)	94.58(1)	105.274(2)	106.327(2)
γ (°)	90	111.253(2)	111.723(2)
V(Å^3)	2261.2(3)	1518.0(3)	1489.8(4)

Crystal Growth

Block-shaped crystals of $Li_2Mn_2(tbaoac)_6$ (**1**) suitable for structural measurements were obtained by keeping its saturated dichloromethane solution at around -20 °C for 2 days.

crystallization temp (°C)	-20
crystal growth method/solvent	solution/dichloromethane
color	colorless
shape	block

Table S2. Crystal Growth of Molecular Precursor 1

X-ray crystallographic procedures

The crystal of $Li_2Mn_2(tbaoac)_6$ (**1**) was immersed in cryo-oil, mounted on a glass fiber, and measured at a temperature of 100(2) K. Its X-ray diffraction data were collected on a Huber Kappa system with a DECTRIS PILATUS3 X 2M(CdTe) pixel array detector using ϕ scans (synchrotron radiation at λ = 0.41328 Å) located at the Advanced Photon Source, Argonne National Laboratory (NSF's ChemMatCARS, Sector 15, Beamline 15-ID-D). Data reduction and integration were performed with the Bruker software package SAINT (version 8.38A).[1] The data were corrected for absorption effects using the empirical methods as implemented in SADABS (version 2016/2).[2] The structure was solved using the intrinsic phasing by SHELXT (version 2018/2)[3] and refined by full-matrix least-squares procedures using the SHELXL (version 2018/3)[4] software package through the OLEX2[5] graphical interface. All non-hydrogen atoms were refined anisotropically. All hydrogen atoms were included at calculated positions and refined as riders with U_{iso}(H) = 1.2 U_{eq}(C) and U_{iso}(H) = 1.5 U_{eq}(C) for methyl groups. Crystallographic data and details of the data collection and structure refinement are listed in Table S3.

Table S3. Crystal Data and Structure Refinement Parameters of $Li_2Mn_2(tbaoac)_6$ (1)

Compound	**1**
Empirical formula	$C_{48}H_{78}Li_2Mn_2O_{12}$
Formula weight	1066.86
Temperature (K)	100(2)
Wavelength (Å)	0.41328
Crystal system	Triclinic
Space group	*P-1*
a (Å)	11.7394(6)
b (Å)	12.2998(7)
c (Å)	12.5347(7)
α (°)	103.9740(10)
β (°)	106.2210 (10)
γ (°)	111.7240(10)
V (Å^3)	1488.88 (14)
Z	1
ρ_{calcd} (g·cm^{-3})	1.190
μ (mm^{-1})	0.124
F(000)	566
Crystal size (mm)	0.029x0.022x0.015
θ range for data collection (°)	1.124-20.164
Reflections collected	13406
Independent reflections	12484
	[R_{int}[a] = 0.0690]
Transmission factors (min/max)	0.7895/0.8564
Data/restraints/params.	13406/0/329
*R*1,[b] *wR*2[c] ($I > 2\sigma(I)$)	0.0373, 0.1023

$R1$,[b] $wR2$[c] (all data)	0.0389, 0.1041
Quality-of-fit[d]	1.054

[a]$R_{int} = \Sigma|F_o^2 - \langle F_o^2 \rangle|/\Sigma|F_o^2|$

[b]$R1 = \Sigma||F_o| - |F_c||/\Sigma|F_o|$. [c]$wR2 = [\Sigma[w(F_o^2 - F_c^2)^2]/\Sigma[w(F_o^2)^2]]$.

[d]Quality-of-fit = $[\Sigma[w(F_o^2 - F_c^2)^2]/(N_{obs} - N_{params})]^{1/2}$, based on all data.

Solid state structure of heterometallic precursor 1

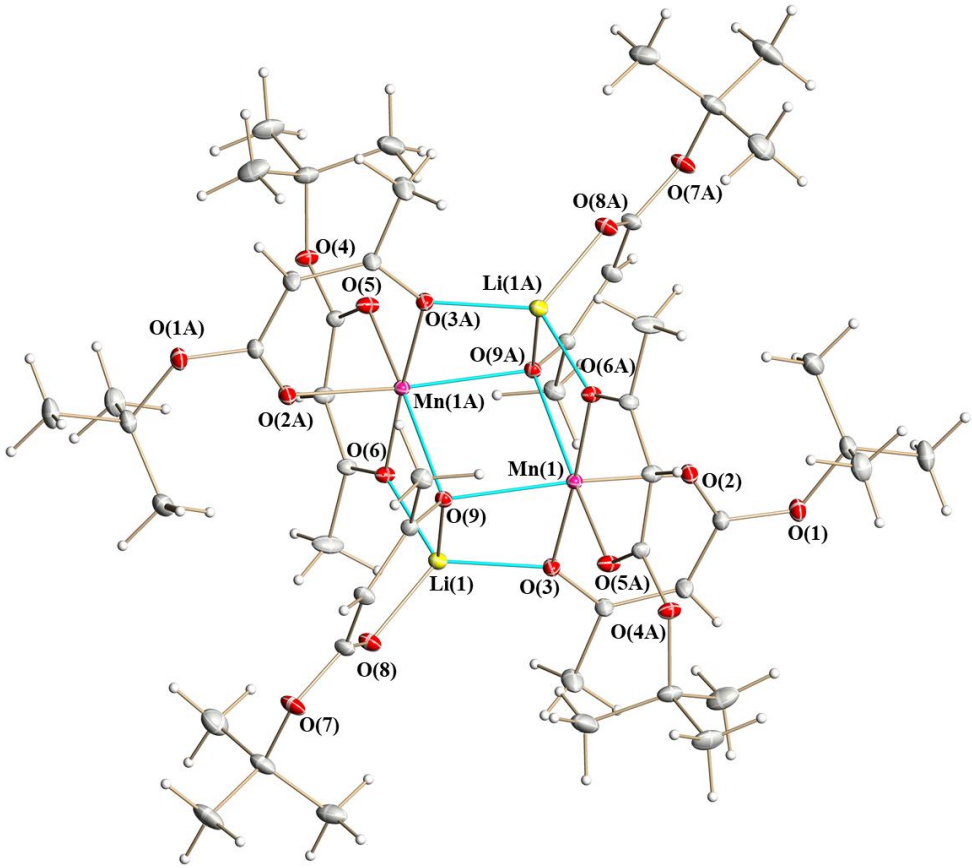

Figure S2. Solid state structure of heterometallic complex $Li_2Mn_2(tbaoac)_6$ (**1**). Atoms are represented by thermal ellipsoids at the 40% probability level. Hydrogen atoms are represented by spheres of arbitrary radius. Only metal and oxygen atoms are labeled. The lithium–oxygen and manganese–oxygen bonds to tbaoac ligands involved in bridging interactions are shown in blue.

Table S4. Selected Bond Distances (Å) and Angles (deg.) in the Structure of $Li_2Mn_2(tbaoac)_6$ (1)

Bond distances		Angles		Angles	
Mn(1)–O(2)	2.1121(5)	O(2)–Mn(1)–O(3)	84.240(19)	O(3)–Li(1)–O(6)	117.84(7)
Mn(1)–O(3)**	2.1337(5)	O(2)–Mn(1)–O(5A)	95.26(2)	O(3)–Li(1)–O(9)	92.36(6)
Mn(1)–O(5A)	2.1225(5)	O(2)–Mn(1)–O(6A)	98.16(2)	O(6)–Li(1)–O(9)	91.98(6)
Mn(1)–O(6A)**	2.1276(5)	O(2)–Mn(1)–O(9)	162.13(2)	O(8)–Li(1)–O(8)	125.91(7)
Mn(1)–O(9)*	2.2211(5)	O(2)–Mn(1)–O(9A)	92.09(2)	O(8)–Li(1)–O(6)	114.57(7)
Mn(1)–O(9A)*	2.2456(5)	O(3)–Mn(1)–O(9)	79.991(18)	O(8)–Li(1)–O(9)	98.42(6)
		O(3)–Mn(1)–O(9A)	99.424(19)		
Li(1)–O(3)*	1.9081(13)	O(5A)–Mn(1)–O(3)	97.18(2)		
Li(1)–O(6)*	1.9109(13)	O(5A)–Mn(1)–O(6A)	83.830(19)		
Li(1)–O(8)	1.8592(13)	O(5A)–Mn(1)–O(9)	94.99(2)		
Li(1)–O(9)**	1.9720(13)	O(5A)–Mn(1)–O(9A)	162.43(2)		
		O(6A)–Mn(1)–O(3)	177.312(18)		
		O(6A)–Mn(1)–O(9)	97.452(19)		
		O(6A)–Mn(1)–O(9A)	79.336(18)		
		O(9)–Mn(1)–O(9A)	82.327(17)		

* – bridging oxygen; ** – chelating-bridging oxygen

ATR-IR spectra of heterometallic precursor 1

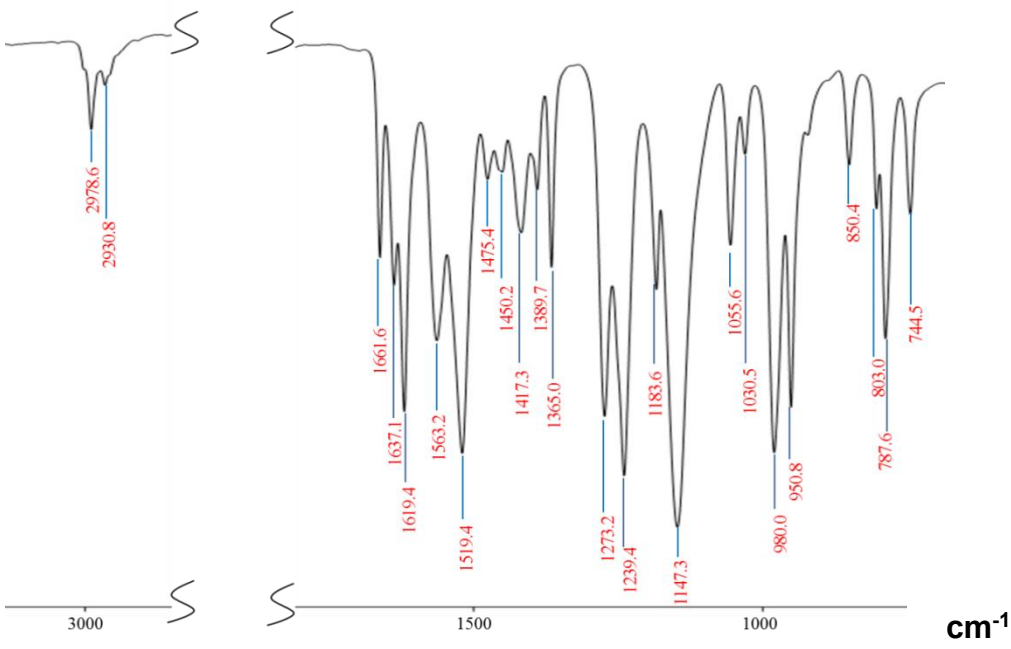

Figure S3. The attenuated total reflection (ATR) spectrum of $Li_2Mn_2(tbaoac)_6$ (**1**)

^{1}H and ^{7}Li NMR spectra of heterometallic precursor 1

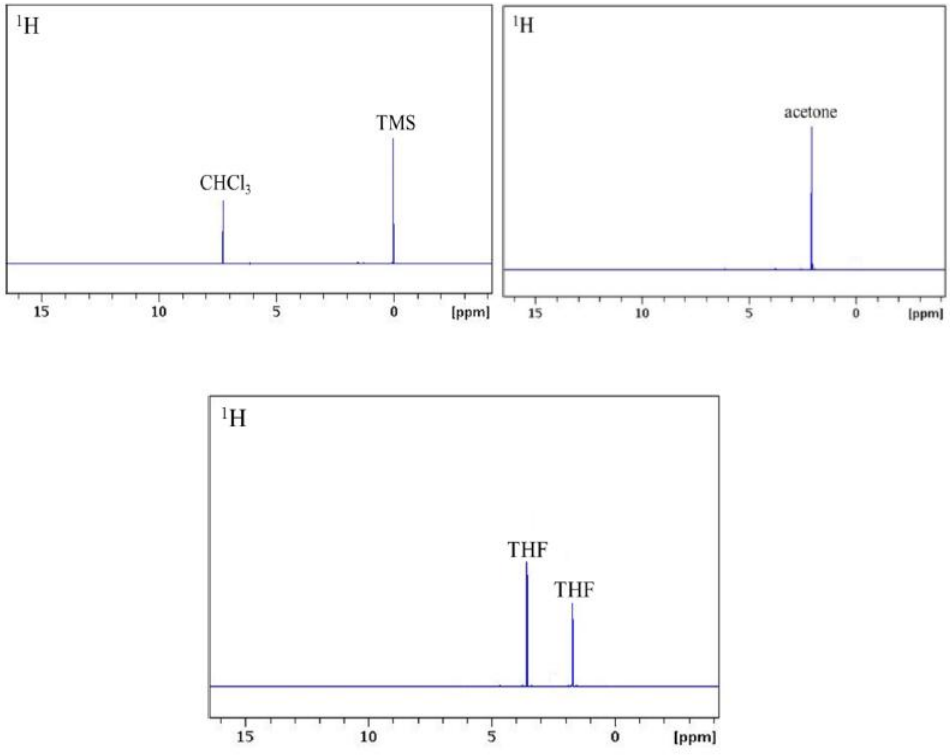

Figure S4. ^{1}H NMR spectra of $Li_2Mn_2(tbaoac)_6$ (**1**) in $CDCl_3$ (top left), d_6-acetone (top right), and d_8-THF (bottom) recorded at room temperature.

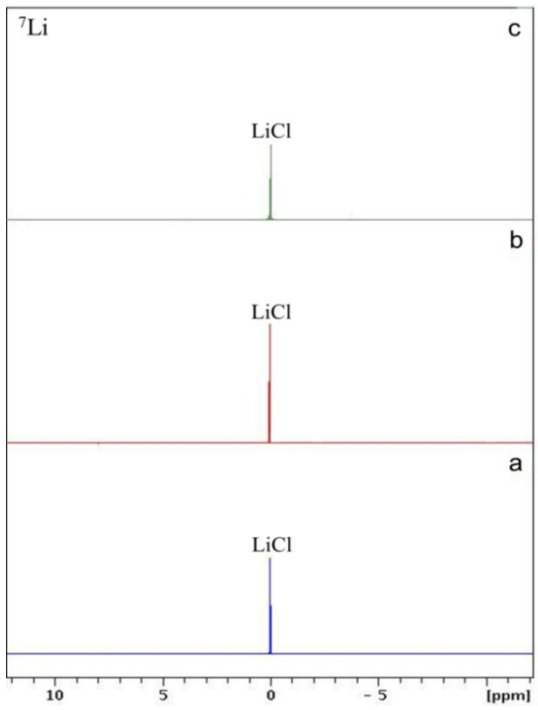

Figure S5. ^{7}Li NMR spectra of $Li_2Mn_2(tbaoac)_6$ (**1**) in (a) $CDCl_3$, (b) d_6-acetone, and (c) d_8-THF recorded at room temperature.

DART mass spectra of heterometallic precursor 1

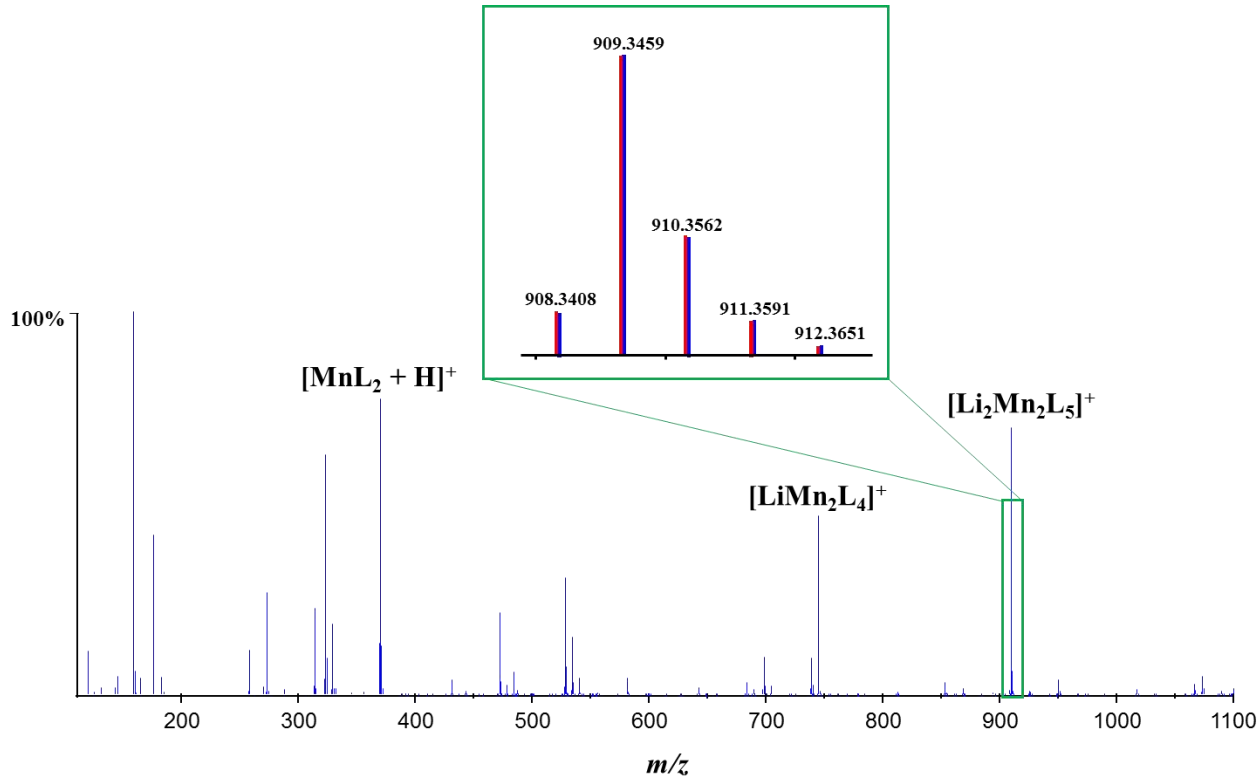

Figure S6. Positive-ion DART mass spectrum of solid $Li_2Mn_2(tbaoac)_6$ (**1**).

Table S5. Assignment of Ions Detected in Positive-Ion DART Mass Spectrum of $Li_2Mn_2(tbaoac)_6$ (1) (M = $Li_2Mn_2(tbaoac)_6$, L = tbaoac = $C_8H_{13}O_3$)

Ions	Measured	Calculated	Δ	Abundance %
$[Li_2Mn_2L_5]^+$	909.3459	909.3404	0.0055	69.87
$[LiMn_2L_4]^+$	745.2420	745.2380	0.0040	47.01
$[Li_2MnL_4+H]^+$	698.3303	698.3238	0.0065	10.28
$[Mn_2L_3]^+$	581.1425	581.1355	0.0070	9.55
$[Li_2MnL_3]^+$	540.2309	540.2294	0.0015	4.93
$[LiMnL_3+H]^+$	534.2239	534.2213	0.0026	15.65
$[LiMnL_2]^+$	376.1316	376.1270	0.0046	3.68
$[MnL_2+H]^+$	370.1201	370.1188	0.0013	77.46
$[Li_2L_2+H]^+$	329.2168	329.2128	0.0040	19.11
$[L+2\ H]^+$	159.1108	159.1021	0.0087	100

Table S6. Isotope Distribution of $[Li_2Mn_2L_5]^+$ Ions Detected in the Positive-ion DART Mass Spectrum of $Li_2Mn_2(tbaoac)_6$ (1)

$[Li_2Mn_2L_5]^+$				
Measured *m/z*	**Calculated *m/z***	**Δ**	**Experimental abundance(%)**	**Theoretical abundance (%)**
908.3408	908.3397	0.0011	15.24	16.03
909.3459	909.3405	0.0054	100	100
910.3526	910.3439	0.0087	41.76	43.36
911.3591	911.3472	0.0119	8.51	9.30
912.3651	912.3506	0.0145	0.95	1.26

Thermal decomposition investigation of molecular precursor 1

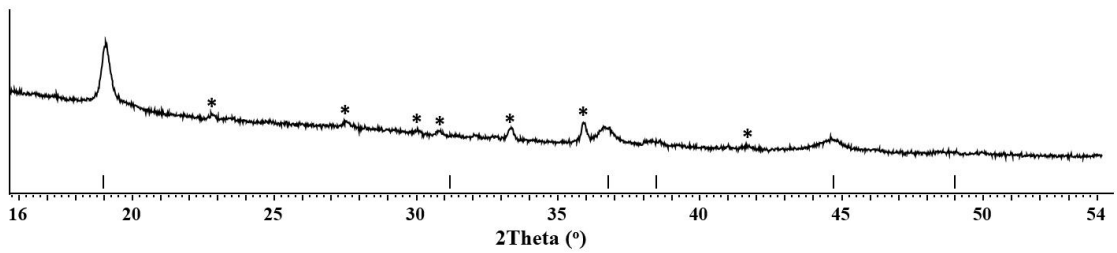

Figure S7. X-ray powder diffraction pattern of thermal decomposition product of heterometallic precursor **1** at 280 °C. Spinel phase peaks are marked as black bars at the bottom, impurity peaks are marked as *. From the Le Bail fit, spinel phase unit cell parameter is a = 8.0990(2) Å.

Electron Microscopy Studies of the $Li_{1.5}Mn_{1.5}O_{3.5}$

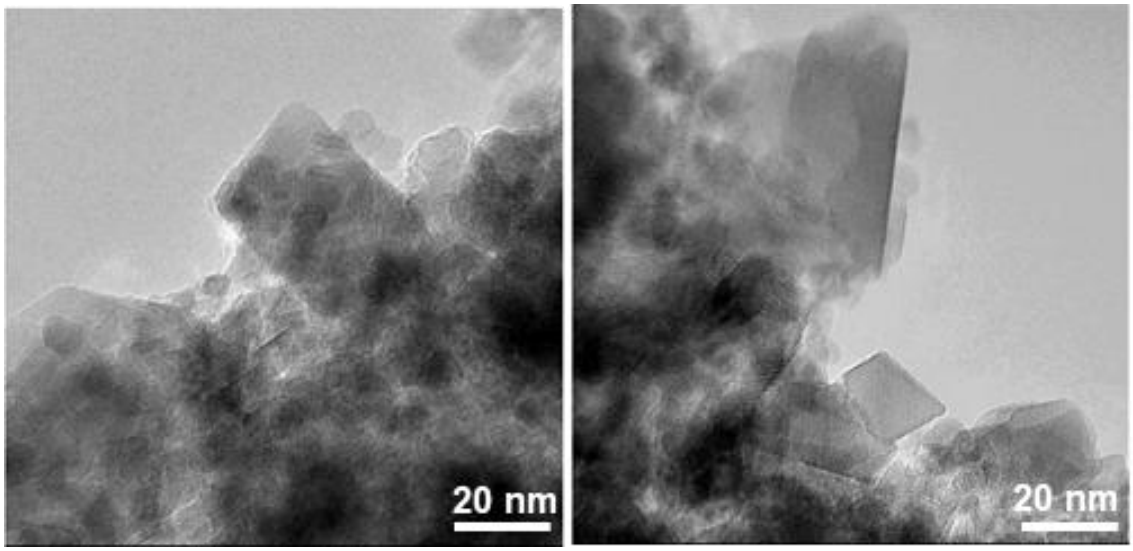

Figure S8. TEM images of $Li_{1.5}Mn_{1.5}O_{3.5}$ obtained by the thermal decomposition of the molecular precursor **1**.

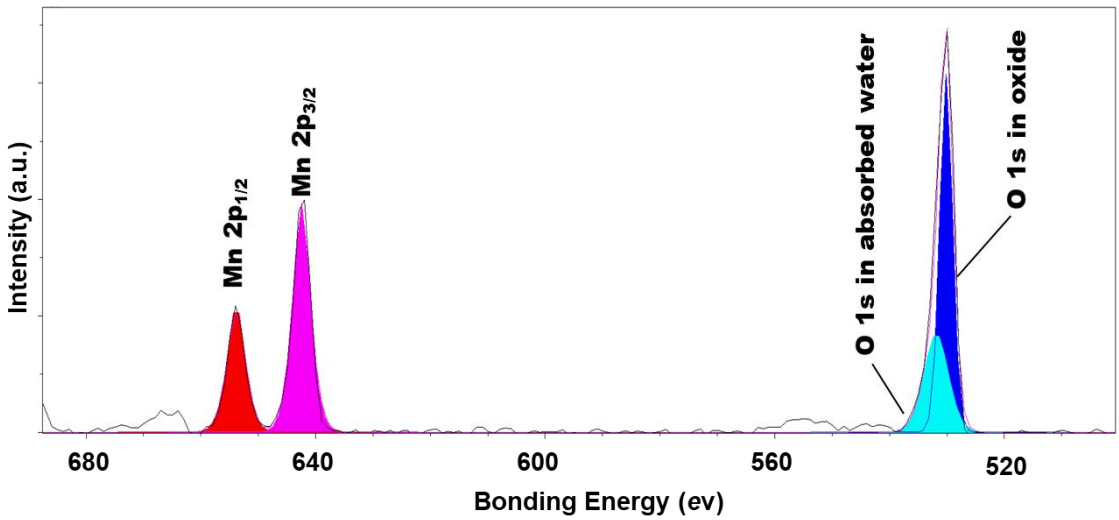

Figure S9. High resolution XPS spectrum of $Li_{1.5}Mn_{1.5}O_{3.5}$. The integration of Mn and O binding energies shows the Mn:O = 1.5:3.5.

Thermal decomposition of metastable $Li_{1.5}Mn_{1.5}O_{3.5}$

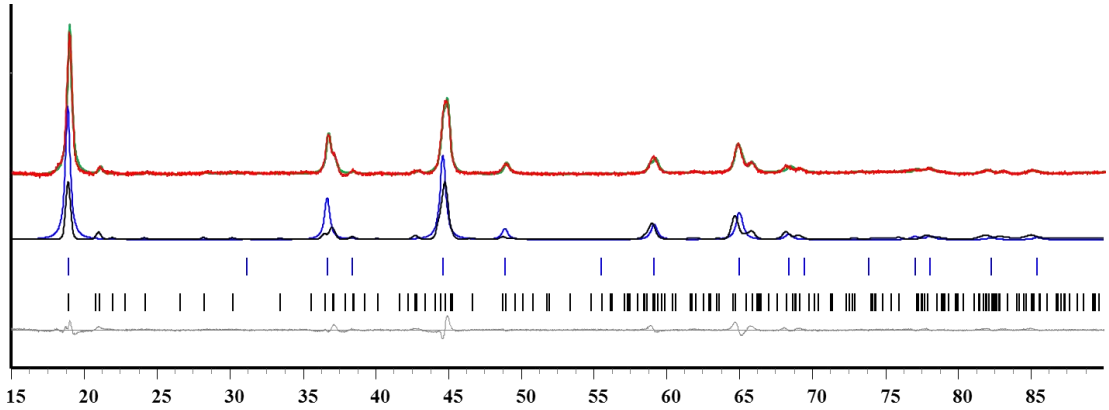

Figure S10. X-ray powder diffraction pattern of decomposition residue obtained by thermal decomposition of $Li_{1.5}Mn_{1.5}O_{3.5}$ at 600 °C for 24 hours in air and the Le Bail fit based on the spinel phase (Sp. Gr. *Fd*-3*m*, *a* = 8.1524(2) Å) and Li_2MnO_3.(*C*2/*c*, *a* = 4.9258(1) Å, *b* = 8.5224(1) Å, *c* = 9.6587(1) Å, *β* = 99.226(5) Å). The red and green curses are the experimental and calculated patterns overlaid. The blue and black curves are calculated cubic and monoclinic patterns, respectively. The grey line is the difference curve. Theoretical peak positions are shown at the bottom.

Table S7. Comparison of the Unit Cell Parameters of Residues Obtained by Decomposition of $Li_2Mn_2(tbaoac)_6$ at 600 °C

	Li_2MnO_3[3]		Li-Mn Spinel	
	Literature data	**Le Bail fit data**	**$Li_{1.5}Mn_{1.5}O_{3.5}$**	**Le Bail fit data**
Sp. Gr.	*C*2/*c*		*Fd*-3*m*	
a (Å)	4.921(6)	4.9258(1)	8.1393(2)	8.1524(2)
b (Å)	8.526(3)	8.5224(1)		
c (Å)	9.606(5)	9.6587(1)		
α (deg.)	90	90		
β (deg.)	99.47(5)	99.226(5)		
γ (deg.)	90	90		

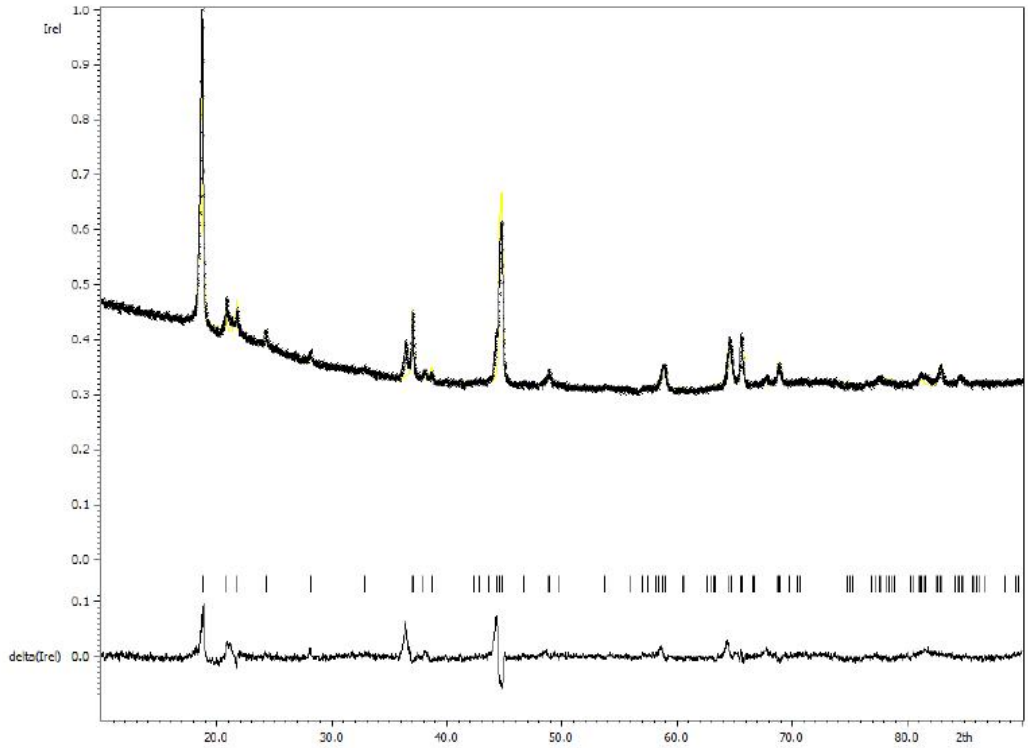

Figure S11. Fitting the powder X-ray diffraction pattern of the decomposition product with the Li_2MnO_3 phase only. Note large residual peaks due to the presence of $LiMn_2O_4$ phase.

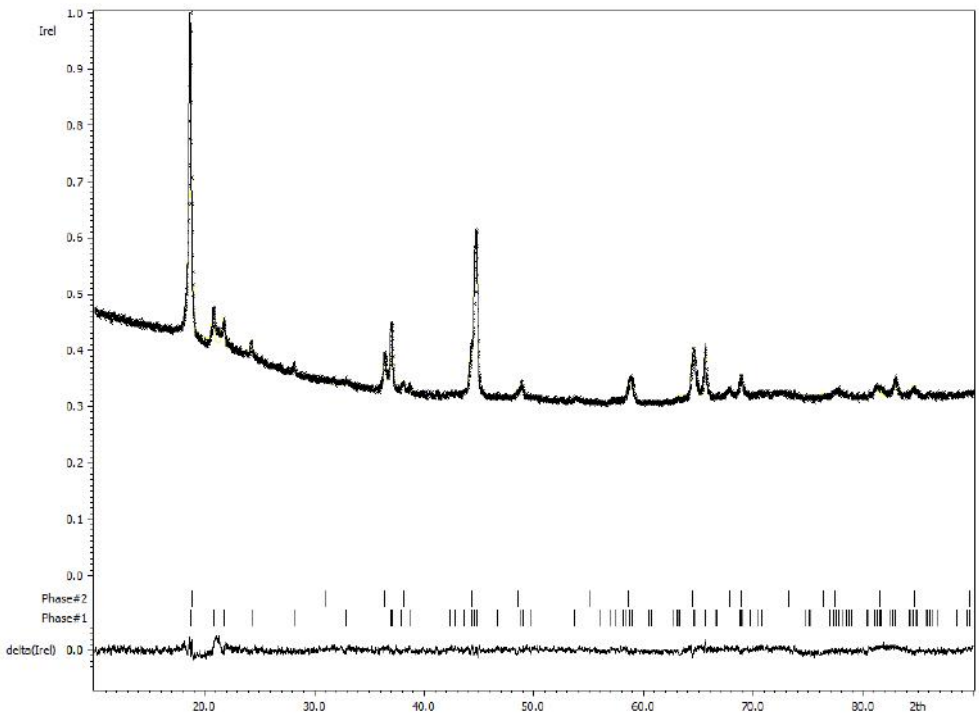

Figure S12. Fitting the powder X-ray diffraction pattern of the decomposition product

with a mixture of Li_2MnO_3 and $LiMn_2O_4$ phases.

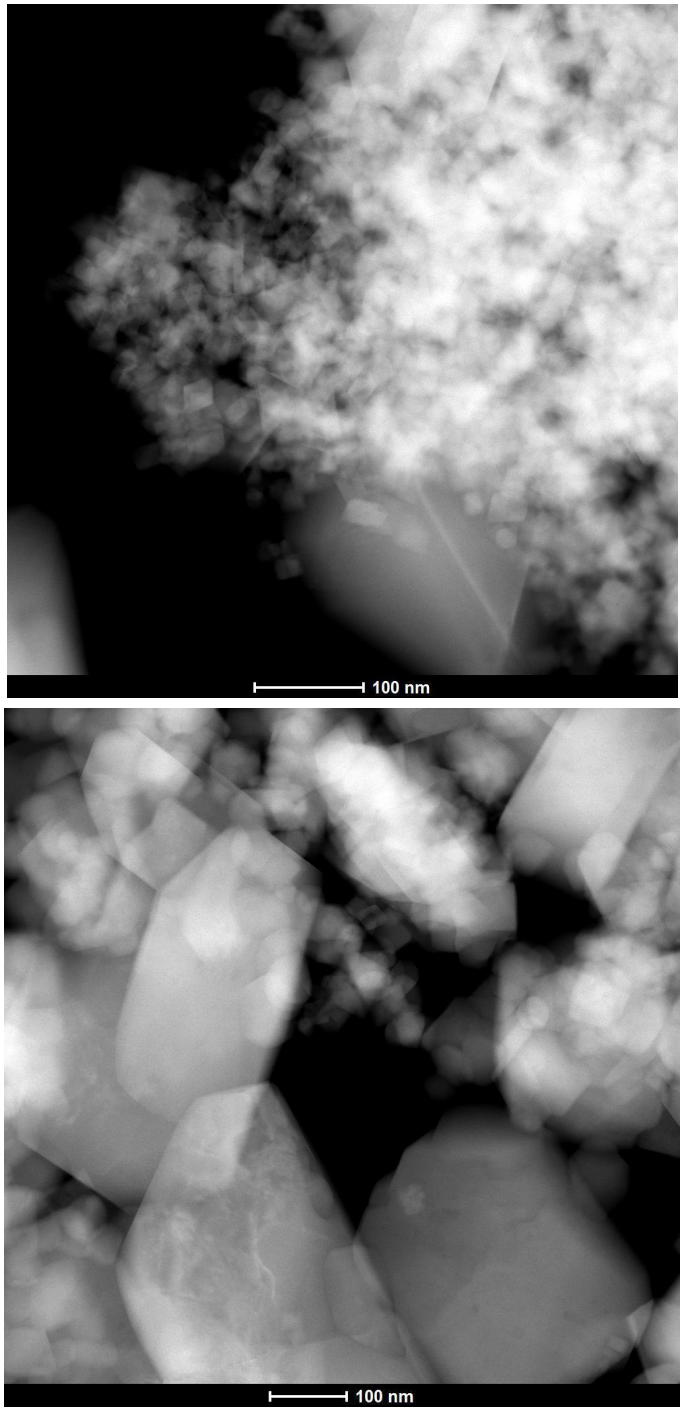

Figure S13. HAADF-STEM images of the crystals obtained by the thermal decomposition of $Li_{1.5}Mn_{1.5}O_{3.5}$ at 600 °C.

Li Manganates

Table S8. Comparison of the Structures, Thermal Stability, and Electrochemical Properties of New Phase with Li Manganates.

	$Li_{1.5}Mn_{1.5}O_{3.5}$	**$LiMn_2O_4$**	**Li_2MnO_3**	**$LiMnO_2$**	**$Li_4Mn_5O_{12}$[b]**	**$Li_4Mn_2O_5$**
Structure Type	Spinel	Spinel	Layered	Layered	Spinel	Rock-salt
Space Group	*Fd*-3*m*	*Fd*-3*m*	*C*2/*m*	*Pmmn*[a]	*Fd*-3*m*	*Cmmm*
Unit Cell Parameters	a = 8.1170(1) Å	a = 8.2211(4) Å	a = 4.9298(4) Å, b = 8.5276(6) Å, c = 5.0223(4) Å, β = 109.333(5) °	a = 4.5725(1) Å, b = 5.7419(2) Å, c = 2.8037(1) Å	a = 8.1616(5) Å	a = 4.0390 Å, b = 12.4312 Å, c = 4.0268 Å
Li:Mn Ratio	1:1	1:2	2:1	1:1	1:1.25	2:1
Mn Oxidation State	+3.67	+3.5	+4	+3	+4	+3
Color	black	black	red	black	black	black
Thermal Stability	< 400 °C	≥ 600 °C	900 °C	≥ 400 °C	≥ 530 °C	≥ 1077 °C
Voltage (*vs* Li/Li^+)	2.75 - 3.20 V	3.5-4.3 V	> 4.5V	2.5-3.0 V	2.3-3.3 V	2.5-4.3 V
Structure	Octahedral: Mn, Li; Tetrahedral: Li	Octahedral: Mn; Tetrahedral: Li	Octahedral: Mn, Li	Octahedral: Mn, Li	Octahedral: Mn; Tetrahedral: Li	Octahedral: Mn; Tetrahedral: Li

[a] Monoclinic modification is also reported; [b] also reported as $Li_{1.33}Mn_{1.67}O_4$.

References

1. SAINT; part of Bruker APEX3 software package (version 2017.3-0): Bruker AXS, **2017**.

2.SADABS; part of Bruker APEX3 software package (version 2017.3-0): Bruker AXS, **2017**.

3. G. M. Sheldrick, *Acta Crystallogr.* **2015**, *A71*, 3-8.

4. G. M. Sheldrick, *Acta Crystallogr.* **2015**, *C71*, 3-8.

5. O. V. Dolomanov, L. J. Bourhis, R. J. Gildea, J. A. K. Howard, H. Puschmann, *J. Appl. Crystallogr.* **2009**, *42*, 339-341.